NADPH oxidase activation is required for pentylenetetrazole kindling-induced hippocampal autophagy

Xinjian Zhu, Kai Shen, Ying Bai, Aifeng Zhang, Zhengrong Xia, Jie Chao, Honghong Yao

www.elsevier.com

PII: S0891-5849(16)00100-3
DOI: http://dx.doi.org/10.1016/j.freeradbiomed.2016.03.004
Reference: FRB12781

To appear in: *Free Radical Biology and Medicine*

Received date: 29 October 2015
Revised date: 19 February 2016
Accepted date: 7 March 2016

Cite this article as: Xinjian Zhu, Kai Shen, Ying Bai, Aifeng Zhang, Zhengrong Xia, Jie Chao and Honghong Yao, NADPH oxidase activation is required for pentylenetetrazole kindling-induced hippocampal autophagy, *Free Radical Biology and Medicine,* http://dx.doi.org/10.1016/j.freeradbiomed.2016.03.004

NADPH oxidase activation is required for pentylenetetrazole kindling-induced hippocampal autophagy

Xinjian Zhu[1*], Kai Shen[1], Ying Bai[1], Aifeng Zhang[3], Zhengrong Xia[4], Jie Chao[2], Honghong Yao[1]

[1] Department of Pharmacology, Medical School of Southeast University, Nanjing, China

[2] Department of Physiology, Medical School of Southeast University, Nanjing, China

[3] Department of Pathology, Medical School of Southeast University, Nanjing, China

[4] Analysis and Test Center of Nanjing Medical University, Nanjing, China

***** Corresponding Author: Xinjian Zhu, Ph.D, Department of Pharmacology, Medical School of Southeast University, 87th Dingjiaqiao Road, Nanjing, China 210029, Tel: 86-25-83272525, Email: xinjianzhu@seu.edu.cn

Abbreviations

Pentylenetetrazole, PTZ

Autophagy-related protein, ATG

Microtubule−associated protein light chain 3, LC-3

Reactive oxygen species, ROS

Dihydroethidium, DHE

Malondialdehyde, MDA

4-hydroxy-2-nonenal, 4HNE

Abstract:

Growing evidence indicates that alterations in autophagy are present in a variety of neurological disorders, ranging from neurodegenerative diseases to acute neurological insults. Only recently has the role of autophagy in epilepsy started to be recognized. In this study, we used pentylenetetrazole (PTZ) kindling, which provides a model of chronic epilepsy, to investigate the involvement of autophagy in the hippocampus and the possible mechanisms involved. Our western blot results showed that autophagy-related proteinswere significantly increased after the mice were fully kindled. In addition, immunofluorescence studies revealed a significant increase in the punctate accumulation of LC3

in the hippocampal CA1 region of fully PTZ-kindled mice. Consistent with the upregulation of ATG proteins and punctate accumulation of LC3 in the hippocampal CA1 region, autophagosomal vacuole formation was observed by an ultrastructural analysis, verifying the presence of a hippocampal autophagic response in PTZ-kindled mice. Increased oxidative stress has been postulated to play an important role in the pathogenesis of a number of neurological diseases, including epilepsy. In this study, we demonstrate that PTZ kindling induced reactive oxygen species (ROS) production and lipid peroxidation, which were accompanied by mitochondrial ultrastructural damage due to the activation of NADPH oxidase. Pharmacological inhibition of NADPH oxidase by apocynin significantly suppressed the oxidative stress and ameliorated the hippocampal autophagy in PTZ-kindled mice. Interestingly, pharmacological induction of autophagy suppressed PTZ-kindling progress and reduced PTZ-kindling-induced oxidative stress while inhibition of autophagy accelerated PTZ kindling progress and increased PTZ-kindling-induced oxidative stress. These results suggest that the oxidative stress induced by NADPH oxidase activation may play a pivotal role in PTZ-kindling process as well as in PTZ kindling-induced hippocampal CA1 autophagy.

Key words:

PTZ kindling; epilepsy; NADPH oxidase; ROS; autophagy

1. Introduction

Autophagy is a catalytic process by which cytoplasmic macromolecules and organelles are degraded and plays an essential role in maintaining cellular homeostasis (Levine and Klionsky, 2004). The initiation of autophagy involves the formation of double-membrane vesicles, named autophagosomes, which subsequently fuse with lysosomes to degrade the contents (Shintani and Klionsky, 2004). Although normal autophagy is required to maintain cellular homeostasis, excessive autophagy may be associated with cell death (Koike et al., 2008, Levine and Kroemer, 2008, Essick and Sam, 2010).

The regulation of autophagy is dependent on several autophagy-related genes (ATG), which are characterized by a high degree of conservation among species as distant as humans and yeast (Klionsky, 2005). Several ATG proteins, such as ATG-5 and ATG-7, are directly involved in the formation of the autophagosome (Ohsumi, 2001). Microtubule-associated protein light chain 3 (LC3)

is the mammalian equivalent of yeast ATG-8, and exists in two forms, LC3-I and LC3-II. LC3-I is normally found in the cytosol, whereas the product of its proteolytic maturation, LC3-II, is located in the autophagosomal membranes. Beclin-1 is the mammalian orthologue of yeast ATG-6 and resides in the trans-Golgi network, where it participates in autophagosome formation (Kabeya et al., 2000). A growing body of evidence suggests that autophagy is involved in various central nervous system diseases (Rubinsztein et al., 2005, Chu, 2006, Hara et al., 2006, Komatsu et al., 2006a). Despite increasing studies about the importance of autophagy in various neurological disorders, there have been relatively few studies regarding the role of autophagy in epilepsy. NADPH oxidase is a cytoplasmic enzyme identified in many cell types that transfers an electron from NADPH to molecular oxygen to generate superoxide. It is recognized that NADPH oxidase subunits are also expressed in neurons (Noh and Koh, 2000, Tammariello et al., 2000) Several lines of evidence have indicated that NADPH oxidase-induced oxidative stress is a major inducer of autophagy, which is important for maintaining cellular homeostasis by recycling dysfunctional macromolecules and organelles (Huang and Brumell, 2009, Scherz-Shouval and Elazar, 2011, Ryter et al., 2012). However, little is known about the NADPH-mediated autophagy in

epilepsy. In the present study, we sought to determine how autophagy is regulated in the hippocampus of PTZ-kindled mice and to explore the role of NADPH oxidase further in the regulation of hippocampal autophagy in PTZ-kindled mice.

2. Materials and Methods

2.1 Animals

Male C57/BL6 mice (four weeks old; weighing 19±2 g at the beginning of the experiments) were obtained from the comparative medicine center of Yangzhou University (Yangzhou, China). The animals were housed in plastic cages and kept in a regulated environment (22±1°C) with an artificial 12 h light/dark cycle (lights on from 8:00 A.M. to 8:00 P.M.). Food and tap water were available *ad libitum*. The procedures used to produce the PTZ kindling epilepsy model were approved by the Animal Care and Use Committee of the Medical School of Southeast University. All efforts were made to minimize animal suffering and discomfort and to reduce the number of animals used.

2.2 Drugs

Pentylenetetrazole (PTZ) (Sigma Aldrich) was dissolved in saline.

Apocynin (Sigma Aldrich) and Rapamycin (Sigma Aldrich) were first dissolved in dimethylsulfoxide (DMSO) and then diluted in saline. Chloroquine diphosphate salt (Sigma Aldrich) and leupeptin hemisulfate (Sigma Aldrich) were dissolved in saline.

2.3 Kindling procedure

The kindling epilepsy model was induced as described previously (Zhu et al., 2015). Briefly, mice were intraperitoneally injected with PTZ (35 mg/kg) once every other day for a total of eleven injections (from Day 1 to Day 21) and mice showing more than three consecutive stage 4 seizures were considered to be fully kindled. Mice that received PTZ (35 mg/kg) once every other day for a total of six injections (from Day 1 to Day 11) and showing stage 2 or stage 3 seizures were considered to be partially kindled. Vehicle control animals were injected with saline. The seizure events during the 30 min period after each PTZ injection were observed. The seizure intensity was scored as follows (Schroder et al., 1993, Becker et al., 1995, Mizoguchi et al., 2011): Stage 0, no response; Stage 1, ear and facial twitching; Stage 2, convulsive twitching axially through the body; Stage 3, myoclonic jerks and rearing; Stage 4, turning over onto the side, wild running, and wild jumping; Stage 5, generalized tonic-clonic seizures; and Stage 6, death. To

determine the role of autophagy in PTZ-induced kindling progress, mice received PTZ injection (35mg/kg) alone or Chloroquine (CQ), (20mg/kg) Apocynin (20mg/kg), Rapamycin (15mg/kg) 30min before each PTZ injection once every other day for eleven total injections. The seizure intensity was scored as described above.

2.4 Brain tissue processing

To assess the levels of autophagy-related proteins, NADPH oxidase subunit p47 phox protein, protein carbonyl and lipid peroxidation, the hippocampus was dissected from vehicle control, partially kindled and fully kindled mice. Dissected hippocampal tissues were then snap-frozen and stored at -80°C until use. For the immunocytochemical analyses of LC3 and p47 phox and ROS measurement, the mice were euthanized by an intraperitoneal injection of an overdose of urethane and were transcardially perfused with 100 mL of saline (0.9% w/v NaCl), followed by 50 mL of 4% paraformaldehyde in 0.05 M sodium phosphate (pH=7.4, containing 0.8% NaCl). The mouse brains were removed and post-fixed overnight in 4% paraformaldehyde, then were cryoprotected in 30% sucrose in 1xPBS for 72 hours. Serial coronal hippocampal sections with a thickness of 25 µm were cut using a cryostat (Leica Microsystems, Wetzlar, Germany) and every sixth

section throughout the hippocampus were collected in 1x PBS as free-floating sections and were stored at 4°C for future immunocytochemistry studies as described previously (Zhu et al., 2006).

2.5 Immunocytochemistry and cell counting

The immunocytochemistry studies of LC3 and NADPH oxidase subunit p47phox were performed on free-floating sections as described previously (Zhu et al., 2006). Briefly, the sections were heated (65°C for 50 min) in antigen unmasking solution (2xSSC/formamide), incubated in 2 M HCl (30°C for 30 min), rinsed in 0.1 M boric acid (pH 8.5) for 10 min, incubated in 1% H_2O_2 in PBS for 30 min and blocked in PBS containing 3% normal goat serum, 0.3% (w/v) Triton X-100 and 0.1% BSA (room temperature for 1 hour), followed by incubation with a rabbit monoclonal anti-LC3 B antibody (1:200; Novus, Littleton, CO, USA) or rabbit polyclonal anti-p47phox antibody (anti-NCF1) (1:250; Abcam, Temecula, CA, USA) at 4°C overnight. Subsequently, the sections were incubated with a fluorescent secondary antibody, a TRITC-conjugated goat anti-rabbit antibody (1:200; Cwbiotech, Beijing, China) for LC3B labeling, or with a streptavidin-biotin enzyme complex (SABC) and a DAB kit (Boster, Wuhan, China) for

p47phox labeling. For LC3/NeuN double labeling, the sections were incubated with the rabbit anti-LC3B monoclonal antibody (1:200; Novus, Littleton, CO, USA) and a mouse anti-NeuN monoclonal antibody (1:200; Abcam, Temecula, CA, USA) at 4°C overnight. The sections were then rinsed and incubated with TRITC-conjugated goat-anti rat (1: 150, Cwbiotech, Beijing, China) and FITC-conjugated goat anti-mouse (1:150, Cwbiotech, Beijing, China) secondary antibodies, respectively. The sections were then rinsed and mounted on gelatin-coated slides in DAPI-anti fade mounting medium (SouthernBiotech, Birmingham, Alabama, USA).

To assess the LC3 puncta and count the p47phox-positive cells, the CA1 region of the hippocampus from each animal was captured, and the quantitative analyses of the LC3 puncta and p47phox-positive cells were performed using the Image J software (NIH, Bethesda, MD, USA) as described in our previous study (Zhu et al., 2015). Briefly, six visual fields (0.6 mm^2) of the hippocampal CA1 region were photographed in every sixth section from a series of 25-μm coronal sections throughout the hippocampus. The numbers of LC3 puncta and p47phox-positive cells in each field were counted at a higher magnification (400×). The data are presented as the number of cells per visual field. Double labeling was imaged with a confocal laser scanning microscope (Olympus

LSM-GB200, Japan).

2.6 Western blotting

The dissected hippocampal tissues of the mice were homogenized in tissue lysis buffer (Beyotime, China). After being lysed for 15 min on ice, samples were centrifuged at 12,000 rpm for 15 min. The protein content in each supernatant fraction was determined using a BCA protein assay kit (Pierce, Rockford, IL, USA) and samples containing equivalent amounts of protein were applied to 12% acrylamide denaturing gels (SDS-PAGE). After electrophoresis, the proteins were transferred to nitrocellulose membranes (Amersham, Little Chalfont, UK) using a Bio-Rad mini-protein-III wet transfer unit (Hercules, CA, USA) overnight at 4°C.

The membranes were then incubated with 5% non-fat milk in TBST (10 mmol/l Tris pH=7.6, 150 mmol/L NaCl, 0.01%Tween-20) for 1 hour at room temperature followed by three washes, then were incubated with rabbit anti-LC3B (1:2500; Novus, Littleton, CO, USA), rabbit anti-Beclin-1 (1:2000; Abcam, Temecula, CA, USA), rabbit anti-ATG-5 (1:2000; Abcam, Temecula, CA, USA), rabbit anti-ATG-7 (1:2500; Sigma-aldrich, St. Louis, MO, USA) , rabbit anti-p47phox (anti-NCF1) (1:2500; Abcam, Temecula, CA, USA), rabbit anti-NOX2/gp91phox (1:2500; Abcam, Temecula, CA, USA)

and rabbit anti-NOXA2/p67phox (1:2500; Abcam, Temecula, CA, USA) in TBST overnight at 4°C. After several washes with TBST buffer, the membranes were incubated for 1 hour with HRP-linked secondary antibody (Boster Bioengineering, Wuhan, China) diluted 1:5,000, followed by four washes. The membranes were then processed with enhanced chemiluminescence (ECL) western blot detection reagents (Millipore, Billerica, MA, USA). Signals were digitally captured using a MicroChemi chemiluminescent image analysis system (DNR Bio-imaging Systems, Jerusalem, Israel). Blots were quantified using the Image J software (NIH, Bethesda, MD, USA).

2.7 Detection of reactive oxygen species (ROS)

To detect superoxide production in the brain sections, a cell membrane-permeable superoxide-sensitive fluorescent dye dihydroethidium (DHE) (Sigma-Aldrich, St. Louis, MO, USA) was used as described previously (Banes et al., 2005). Briefly, hippocampal sections were incubated with 1 μM DHE in 0.1 M phosphate buffer (PBS, PH=7.4) at room temperature for 15 min in the dark. The sections were then washed with PBS three times and mounted on gelatin-coated slides. The fluorescence of DHE was visualized by a confocal laser scanning microscope (Olympus LSM-GB200, Japan) using an excitation wavelength of 520 to 540

nm. Fluorescence was quantified with the Image J software program (NIH, Bethesda, MD, USA).

2.8 Measurement of the lipid peroxidation and protein oxidation

The lipid peroxidation was evaluated by detecting the levels of malondialdehyde (MDA) and 4-hydroxy-2-nonenal (4HNE). Briefly, the dissected hippocampal tissues from mice were homogenized in tissue lysis buffer (Beyotime, China). After being lysed for 15 min on ice, the homogenates were centrifuged at 3,000 rpm for 15 min. The protein content in each supernatant fraction was determined using a BCA protein assay as described in the western blotting section above. The levels of MDA and 4-HNE in the supernatant were measured by a commercially available MDA assay kit (Jiancheng Bioengineering, Nanjing China) and 4-HNE assay kit (Cell Biolabs, San Diego, CA), respectively. The MDA content was expressed as nmol per mg protein while the 4-HNE content was expressed as μg per g protein. The extent of protein oxidation was assayed by measuring the protein carbonyl content using a protein carbonyl content assay kit (Sigma Aldrich). The protein carbonyl content was expressed as nmol per mg protein. All assays were conducted according to the manufacturer's instructions.

2.9 Transmission electron microscopy

For the transmission electron microscopy (TEM) analyses, mice were deeply anesthetized and transcardially perfused with 0.1 M phosphate buffer (PBS, pH=7.4), followed by 4% PFA and 2% glutaraldehyde. The CA1 subfield of the hippocampus was then removed and processed for electron microscopy. Tissue samples were diced and immediately submerged in 2.5% glutaraldehyde (0.1 M sodium cacodylate buffer, pH=7.2). Each specimen was trimmed and embedded in Spurr's medium. Tissue blocks were post-fixed with osmium, en bloc stained with uranyl acetate, and post-stained with uranyl acetate and lead citrate. Tissue sections were cut to a thickness of 60-70 nm and viewed on 300-mesh coated grids using a transmission electron microscope (JEOL, JEM-1010, Tokyo, Japan). The images were acquired digitally from a randomly selected pool of eight visual fields (800 μm^2) under each condition. The numbers of autophagosomes were counted and the data are presented as the average number of autophagosomes per visual field.

2.10 Statistical analysis

All data are presented as the means $\pm$ S.E.M. Statistical significance was determined using one-way or two-way ANOVA for

multi-group comparisons, and repeated-measures ANOVA. Tukey's test was used for *post-hoc* comparisons. Differences were considered to be significant for values of $p<0.05$.

3. Results

3.1 PTZ-induced kindling model

The PTZ kindling model was generated by repeatedly and intermittently treating the mice with a sub-convulsive dose of PTZ, as described in our previous study (Zhu et al., 2015). Compared to the vehicle control mice, the mice repeatedly treated with PTZ showed a progressive increase in seizure severity from almost no observable convulsive behaviors to major tonic-clonic seizures. In the partially kindled group, most of the mice developed stage 2 to stage 3 seizures after the final dose. In contrast, in the fully kindled group, almost all of the mice had become kindled by the final dose, with at least three consecutive stage 4 seizures **(Fig. 1).**

3.2 PTZ kindling induced the expression of hippocampal autophagy-related proteins

To investigate whether autophagy is activated in the hippocampus of PTZ kindled mice, we first examined the expression of

ATG-related proteins, including LC3, Beclin-1, ATG-5 and ATG-7, which are key components required for autophagy, at six and 24 hours after the mice were fully kindled **(Fig. 2A).** Our Western blot results revealed that the protein levels of Beclin-1, ATG-5 and ATG-7 in the hippocampus started to increase by six hours after the mice were fully kindled and were significantly elevated 24 hours after the mice were fully kindled **(Figs. 2D-2F)**, whereas none of these ATG-related proteins were increased in the partially kindled mice compared to the vehicle control mice. These findings indicate that the autophagic components are indeed increased in the hippocampus of fully PTZ-kindled mice.

LC3-II is a marker of autophagosomes that is processed from LC3-I and specifically localized in the autophagosomes. The amount of LC3-II and the ratio of LC3-II/ LC3-I therefore correlates with the number of autophagosomes (Kabeya et al., 2000). Our data showed that the level of LC3-II was significantly increased at 24 hours after the mice were fully kindled **(Fig. 2B,)**. Furthermore, the ratio of LC3-II/LC3-I was significantly increased in the PTZ-kindled mice **(Fig. 2C)**. Taken together, these data suggest that PTZ kindling induced the expression of hippocampal autophagy-related proteins.

3.3 PTZ kindling induced the accumulation of autophagosomes in the hippocampal CA1 region

As noted above, LC3 is localized in the autophagosomes, where it forms numerous small puncta (Kabeya et al., 2000). To further characterize the autophagosome formation, we examined the LC3-containing puncta by immunofluorescence. In the vehicle control mice, there was a slight accumulation of LC3 puncta in the hippocampal CA1 region **(Fig. 3A),** indicating a low basal level of autophagy in control animals. However, 24 hours after the mice were fully kindled, a large increase of LC3 puncta accumulation was observed in the hippocampal CA1 region **(Figs. 3C-3F,).** In the partially kindled mice, the LC3 puncta remained similar to those observed in the vehicle control mice **(Figs. 3B, 3F).**

To determine cell type specificity of autophagosome accumulation, we performed co-immunostaining using antibodies against LC3 and a neuronal marker, NeuN. Our results showed that approximately 65% of the LC3 puncta-positive cells were co-labeled with NeuN **(Fig. 3E)**, indicating that the punctate accumulation of LC3 mostly occurred in neurons.

To evaluate the autophagosome formation based on ultrastructural criteria, we performed a transmission electron microscopy (TEM) analysis on the hippocampal CA1 regions of

mouse brains. Consistent with the punctate accumulation of LC3, considerable autophagosome vacuoles were detected in the hippocampal CA1 region of fully PTZ-kindled mice compared to the vehicle control mice **(Figs. 3G, 3H)**. Furthermore, the numbers of autophagosomal vacuoles were significantly increased in the fully kindled mice compared to vehicle control mice **(Fig. 3I)**.

To measure autophagic flux, fully PTZ-kindled and control mice were treated with saline or leupeptin (40mg/kg) to block lysosomal degradation. Mice were then sacrificed 24 hour later and protein from hippocampus was extracted for detection the level of LC3 by western blot **(Fig. 3J)**. Our results showed that levels of LC3-II in leupeptin-treated mice were increased 24 hour after injection as compared with those in control animals **(Fig. 3K)**. This finding indicates that leupeptin can cross the blood brain barrier and block lysosomal activity, demonstrating the existence of basal autophagic flux in the adult mouse hippocampus. PTZ-kindling resulted in an increase in LC3-II levels, an effect that was augmented by concomitant lysosomal inhibition with leupeptin**(Fig. 3K)**. Furthermore, the ratio of LC3-II/LC3-I in leupeptin-treated mice were increased 24 hour after injection as compared with those in control animals **(Fig. 3L)**, PTZ-kindling resulted in an increase in the ratio of LC3-II/LC3-I, which was augmented by concomitant

lysosomal inhibition with leupeptin **(Fig. 3L)**, indicating autophagic flux was induced in the hippocampus of PTZ-kindled mice.Taken together, these data suggest that PTZ kindling induced autophagosome accumulation within the hippocampal CA1 region.

3.4 PTZ kindling induced hippocampal NADPH oxidase activation

It has been reported that NADPH oxidase is involved in the pathological process in the pilocarpine model of temporal lobe epilepsy (Pestana et al., 2010). To explore whether NADPH oxidase is involved in the PTZ kindling epilepsy model, we examined the expression of the key subunit of NADPH oxidase, p47phox, which regulates the activity of the enzyme by assembling the NADPH oxidase functional complex at the membrane (Bedard et al., 2007). Our immunohistological study showed a significant increase in p47phox immunostaining in the CA1 region of the hippocampus after the mice were fully kindled **(Fig. 4A)**. Quantification showed that the number of p47phox-positive cells in hippocampal CA1 region was significantly increased in the fully kindled mice compared to vehicle control mice **(Fig. 4A,)**.

Consistent with the immunohistological data, our Western blot

results revealed that the p47phox protein content in the hippocampus was significantly increased at six and 24 hours after the mice were fully kindled compared to the vehicle control mice **(Fig. 4B)**. However, the expression of other subunits of NADPH oxidase including p67phox and gp91phox remain similar among different group of mice **(Fig. 4B)**. These findings suggested that PTZ kindling induced NADPH oxidase activation in the hippocampal CA1 region.

3.5 PTZ kindling-induced oxidative stress is dependent on the activation of NADPH oxidase

Increased generation of ROS and lipid peroxidation have been suggested to result in oxidative stress. An increasing number of studies have suggested that oxidative stress is involved in the pathogenesis of epilepsy (Liang and Patel, 2004, Peker et al., 2009, Tsai et al., 2010). A recent study by our laboratory found that the MDA level was significantly increased in the PTZ-kindled mice (Zhu et al., 2015).

Apocynin is a well-established NADPH oxidase inhibitor which acts by impeding the assembly of the p47phox and p67phox subunits within the membrane NADPH oxidase complex (Meyer, J. W., 2000), consequently reducing the p47phox membrane

translocation. To determine whether pharmacological inhibition of NADPH oxidase is sufficient to modulate the PTZ kindling-induced oxidative stress in the mouse hippocampus, mice were intraperitoneally injected four times with the NADPH oxidase inhibitor, apocynin (20 mg/kg) every six hours beginning immediately after they were kindled. The mice were then examined for hippocampal ROS production, lipid peroxidation and mitochondrial ultrastructure changes **(Fig. 5A).**

We first examined the hippocampal CA1 ROS accumulation profiles by measuring the DHE-reactive superoxide **(Fig. 5B).** Our data showed that the fully PTZ-kindled mice displayed higher DHE fluorescence intensity compared to the vehicle control mice **(Fig. 5C).** However, pharmacological inhibition of NADPH oxidase by apocynin suppressed the PTZ kindling-induced increase in the DHE intensity **(Fig. 5C)**, while the mice treated with apocynin alone did not show a significant difference in the DHE intensity compared to the vehicle control mice **(Fig. 5C)**.

Next, we examined the lipid peroxidation by detecting lipid peroxidation products MDA and 4-HNE. Our data showed that the MDA content was significantly increased in fully PTZ-kindled mice compared to the vehicle control mice **(Fig. 5D).** However, pharmacological inhibition of NADPH oxidase by apocynin

suppressed the PTZ kindling-induced increase in the MDA level **(Fig. 5D)**, while mice treated with apocynin alone did not show any significant difference in the MDA content compared to the vehicle control mice **(Fig. 5D)**. 4-HNE content was significantly increased in fully PTZ-kindled mice compared to the vehicle control mice **(Fig. 5E).** Pharmacological inhibition of NADPH oxidase by apocynin suppressed the PTZ kindling-induced increase in the 4-HNE level **(Fig. 5E)**, while the mice treated with apocynin alone did not show any significant difference in the 4-HNE content compared to the vehicle control mice **(Fig. 5E)**. Taken together, these data suggest that the PTZ kindling-induced oxidative stress is dependent on the activation of NADPH oxidase.

3.6 PTZ kindling induced mitochondrial ultrastructural damage in the hippocampal CA1 region

It is generally accepted that cellular changes occur as a consequence of epileptic seizures and may play an important role in the epilepsy-associated pathological processes. A recent study reported that an increased level of oxidative stress was associated with impaired mitochondrial function in epilepsy (Rowley et al., 2015). In the present study, we specifically investigated the ultrastructural changes of the mitochondria in the hippocampal CA1

region by transmission electron microscopy (TEM) 24 hours after the mice were fully kindled. In the vehicle control mice, the mitochondria were normal, and maintained intact inner and outer membranes, clear cristae and a smooth matrix **(Fig. 6A)**. In contrast, the mitochondria in fully PTZ-kindled mice displayed swelling, dilation, outer membrane ruptures and cristae disruption **(Fig. 6B)**. The administration of apocynin ameliorated PTZ kindling-induced mitochondrial ultrastructure damage. As seen in **Fig. 6C,** the mitochondria were slightly swollen, with mild cristae and inner and outer membrane disruption in the apocynin-treated PTZ-kindled mice. The mitochondria in the mice treated with apocynin alone maintained intact membranes, clear cristae and a smooth matrix, which were similar to those of vehicle control mice **(Fig. 6D)**. These data suggest that the PTZ kindling-induced mitochondria ultrastructural damage is dependent on the activation of NADPH oxidase.

3.7 PTZ kindling-induced hippocampal autophagy is dependent on the activation of NADPH oxidase

To further investigate whether PTZ kindling-induced hippocampal autophagy is dependent on the activation of NADPH oxidase, we treated mice with apocynin (20mg/kg) to pharmacologically inhibit

NADPH oxidase activity after they were fully kindled **(Fig. 5A)** and examined the level of autophagy in the hippocampus. Western blotting showed that the PTZ kindling-induced expression of hippocampal autophagy-related proteins, such as LC3-II, Beclin-1, ATG-5 and ATG-7, was suppressed by inhibiting NADPH oxidase with apocynin **(Fig. 7A).** A quantitative study revealed that apocynin treatment significantly decreased the PTZ kindling-induced levels of the LC3-II **(Fig. 7B)**, Beclin-1 **(Fig. 7D)**, ATG-5 **(Fig. 7E),** and ATG-7 **(Fig. 7F)** proteins and the ratio of LC3-II/ LC3-I **(Fig. 7C).** Furthermore, our immunofluorescence study showed that the increase in punctate LC3 accumulation in the hippocampal CA1 region of PTZ-kindled mice was suppressed by inhibition of NADPH oxidase with apocynin **(Figs. 7G).** Moreover, a quantitative study revealed that apocynin treatment significantly decreased the number of LC3 puncta-positive cells in fully kindled mice **(Fig. 7I)**. An ultrastructural TEM analysis revealed that considerable numbers of autophagosomal vacuoles were formed in the hippocampal CA1 region 24 hours after the mice were kindled **(Fig. 7F)**. However, the administration of apocynin significantly decreased the number of autophagosomal vacuoles in fully kindled mice **(Figs. 7J,)**. Taken together, these findings suggest that the PTZ kindling-induced hippocampal autophagy is dependent on the

activation of NADPH oxidase.

3.8 Pharmacological modulation of autophagy alters PTZ-induced kindling development

To determine the role of autophagy in PTZ-induced kindling process, we treated mice with pharmacological inducer and inhibitor of autophagy before each single PTZ treatment. Our results showed that induction of autophagy by rapamycin (Rapamycin+PTZ) suppressed kindling development, while inhibition of autophagy by CQ (CQ+PTZ) accelerated kindling development **(Fig. 8A)**. In addition, inhibition of NADPH oxidase by Apocynin (Apocynin+PTZ) also suppressed kindling development **(Fig. 8A)**.

To further determine the oxidative stress status and their relationship with autophagy during PTZ-induced kindling progress, we detected protein oxidation and lipid peroxidation level 30 minutes after the last injection of PTZ in PTZ, CQ+PTZ, Rapamycin+PTZ and Apocynin+PTZ mice respectively. Our results showed that inhibition of autophagy by CQ during PTZ-inducing kindling process increased the protein carbonyl content which is an indicator of protein oxidation **(Fig. 8B)** and the level of 4-HNE which is an indicator of lipid peroxidation **(Fig.8C)**, while induction of

autophagy by rapamycin decreased protein carbonyl content **(Fig. 8B)** and level of MDA which is another indicator of lipid peroxidation **(Fig. 8D)**. Moreover, inhibition of NADPH oxidase by apocynin during PTZ-inducing kindling process decreased protein carbonyl content **(Fig. 8B)** and 4-HNE level **(Fig. 8C)**. Taken together, these results suggest that pharmacological induction of autophagy suppressed PTZ-kindling progress and reduced PTZ-kindling-induced oxidative stress while inhibition of autophagy accelerated PTZ kindling progress and exacerbate PTZ-kindling-induced oxidative stress.

4. Discussion

In this study, we demonstrated that PTZ kindling induced autophagy in the hippocampal CA1 region, and this PTZ kindling-induced autophagy was accompanied by increased reactive oxygen species (ROS) production, lipid peroxidation and mitochondrial injuries through the activation of NADPH oxidase. Inhibition of NADPH oxidase suppressed the PTZ kindling-induced oxidative stress and decreased the hippocampal autophagy in

PTZ-kindled mice. Interestingly, pharmacological induction of autophagy suppressed PTZ-kindling progress and reduced PTZ-kindling-induced oxidative stress while inhibition of autophagy accelerated PTZ kindling progress and increased PTZ-kindling-induced oxidative stress. Overall, our study suggests that NADPH oxidase-related oxidative stress may play a pivotal role in PTZ kindling-induced hippocampal CA1 autophagy as well as in PTZ-kindling progress.

Autophagy is a key catabolic process that is responsible for the recycling and degradation of proteins and organelles through the lysosomal machinery, and has been linked to diverse neurological diseases (Levine and Kroemer, 2008). The role of autophagy in epilepsy has gained increasing attention due to the finding that rapamycin, a powerful inducer of autophagy (Rangaraju et al., 2010), strongly affects various models of seizure and epilepsy (McMahon et al., 2012, Siebel et al., 2015, Sosanya et al., 2015).

Two early studies reported that hippocampal autophagy was increased in kainic acid-induced seizure (Shacka et al., 2007) and in pilocarpine-induced status epilepticus (SE) models (Cao et al., 2009). Consistent with these reports, we found an increase in the hippocampal CA1 autophagy level, as measured by the expression of autophagy-related proteins, in the PTZ kindling epilepsy model

(Figs. 2A-2F). This suggests that PTZ kindling induces hippocampal CA1 autophagy. This is further supported by the finding that the punctate accumulation of LC3 **(Figs. 3A-3F)** and the formation of autophagosome vacuoles were increased in the hippocampal CA1 region of PTZ-kindled mice **(Figs. 3G-3I)**.

Although there is little detectable autophagy in the normal mature mammalian brain (Mizushima et al., 2004), disrupting the autophagic process in the brain is deleterious, resulting in the accumulation of dysfunctional or aging macromolecules and organelles. Autophagy-deficient mice, including Atg3, Atg5, or Atg7 knockout mice, die shortly after birth (Komatsu et al., 2005, Komatsu et al., 2006b), indicating that autophagy is an important homeostatic process involved in eliminating toxic protein aggregates, defective organelles and pathogens from cells. Increased autophagy has now been reported in experimental models of traumatic brain injury (TBI), cerebral ischemia, excitotoxicity and epilepsy (Degterev et al., 2005, Zhu et al., 2005, Shacka et al., 2007, Lai et al., 2008, Cao et al., 2009), suggesting that autophagy is upregulated in response to various neurological insults and is likely a component of excitotoxicity, which contributes to cell death (Martin and Baehrecke, 2004, Crighton et al., 2006, Espert et al., 2006).

Autophagy can be induced by a variety of stimuli under different conditions. Reactive oxygen species (ROS) have been considered to be important autophagic activators (Scherz-Shouval and Elazar, 2007, Scherz-Shouval et al., 2007). NADPH oxidase is a major source of ROS production in various cell types (Lambeth, 2004, Bedard and Krause, 2007) because it transfers electrons from NADPH in the cytosol across a membrane to oxygen molecules, generating superoxide ions (O_2^-), which can be rapidly converted to ROS (Nauseef, 2008).

A growing body of evidence suggests that NADPH oxidase is responsible for epilepsy-associated oxidative stress (Pestana et al., 2010, Di Maio et al., 2011, Kim et al., 2013, Kovac et al., 2014). In this study, we found that PTZ kindling activated NADPH oxidase **(Figs. 4A, 4B)** and promoted the generation of ROS and lipid peroxidation **(Figs. 5B-5E),** which is consistent with our previous data (Zhu et al., 2015). Inhibiting NADPH oxidase suppressed the PTZ kindling-induced ROS generation and lipid peroxidation **(Figs. 5B-5E)**, indicating that the PTZ kindling-induced oxidative stress is dependent on the activation of NADPH oxidase.

Previous studies reported that the activity of NADPH oxidase and the ROS generated are key signals that induce autophagy (Huang and Brumell, 2009, Huang et al., 2009). Consistent with this

idea, we herein demonstrated that the pharmacological inhibition of NADPH oxidase suppressed PTZ kindling-induced autophagy **(Figs. 7A-7I)**. Thus, the NADPH oxidase activity-dependent oxidative stress, including ROS generation and lipid peroxidation, appear to be essential for PTZ kindling-induced autophagy.

Mitochondria are intracellular organelles enclosed by a double membrane-bound structure. The primary function of mitochondria is the production of cellular energy in the form of adenosine triphosphate (ATP) through the mitochondrial respiratory chain. Multiple lines of evidence support a role for mitochondria in the pathological process(es) associated with epilepsy (Waldbaum et al., 2010, Ryan et al., 2012, Ryan et al., 2014). It is believed that mitochondria are the main targets of oxidative stress. A recent study reported that deficits in mitochondrial respiration were driven by ROS in experimental temporal lobe epilepsy (Rowley et al., 2015). A loss of mitochondrial membrane potential and mitochondrial impairment have been linked to autophagy (Itoh et al., 2008Itoh et al., 2008, Lee et al., 2012).

Consistent with these studies, we found that the mitochondria in the hippocampal CA1 region undergo ultrastructural injuries after PTZ-induced kindling, which were manifested by outer membrane rupture and cristae disruption **(Fig. 6B)**. Interestingly, this PTZ

kindling-induced mitochondrial ultrastructure damage was ameliorated by inhibiting NADPH oxidase **(Fig. 6C)**, implying that mitochondrial injuries are an important link between oxidative stress and autophagy due to the activation of NADPH oxidase in the PTZ-kindled epilepsy model.

It is believed that autophagy plays an important role in the development of epilepsy. We herein demonstrated that pharmacological induction of autophagy suppressed PTZ-kindling progress and reduced PTZ-kindling-induced oxidative stress while inhibition of autophagy accelerated PTZ-kindling progress and exacerbated PTZ-kindling-induced oxidative stress **(Figs. 8A-8D)**. Combined with the findings that autophagy is stimulated during PTZ-induced kindling process, these results suggested that enhanced autophagy during PTZ-induced kindling process may reflect a compensatory attempt, although unsuccessful, to remove the misfolded or aggregated proteins and damaged organelles caused by oxidative stress in this process and to relieve the neuronal excitability. Enhancement of autophagy by Rapamycin during kindling process facilitated to remove aggregated proteins and damaged organelles and significantly relieved the neuronal excitability, which consequently suppressed the kindling development. On the contrary, inhibition of autophagy by CQ during

kindling process suppressed the clearance of aggregated proteins and damaged organelles and increased the neuronal excitatory toxicity, which consequently accelerated the kindling development. Furthermore, the accumulation of misfolded or aggregated proteins and damaged organelles caused by oxidative stress during kindling development may overwhelm the capacity of the clearance of oxidative species, therefore, eventually creating a vicious cycle and accelerated kindling progress. In agreement with this hypothesis, our results showed that inhibition of autophagy by CQ increased the protein carbonyl content and the 4-HNE level, while induction of autophagy by rapamycin decreased protein carbonyl content and MDA level **(Fig.8B-8D)**. In addition, we found that inhibition of NADPH oxidase by apocynin during PTZ-inducing process also suppressed kindling development and reduced protein carbonyl content and MDA level, suggesting oxidative stress may contribute to the development of kindling **(Fig. 8A-8D)**.

In conclusion, the present findings demonstrate that PTZ kindling induced reactive oxygen species (ROS) production and lipid peroxidation, which were accompanied by mitochondrial injuries resulting from the activation of NADPH oxidase. Inhibition of NADPH oxidase activity suppressed the oxidative stress and

ameliorated the hippocampal autophagy in PTZ-kindled mice. Moreover, induction of autophagy suppressed PTZ-kindling progress and reduced oxidative stress while inhibition of autophagy accelerated PTZ kindling progress and increased oxidative stress. These data suggest that NADPH oxidase activation-induced oxidative stress may play a pivotal role in PTZ-induced kindling process as well as in PTZ kindling-induced autophagy in the hippocampal CA1 region.

Conflict of Interest Disclosure:

The authors declare no competing financial interests.

Acknowledgments:

This work was supported by grants from the Natural Science Foundation of Jiangsu Province (BK20141335 to Xinjian Zhu), the Specialized Research Fund for the Doctoral Program of Higher Education (20130092120043 to Xinjian Zhu) and the Scientific Research Foundation of the State Education Ministry for the Returned Overseas Chinese Scholars (No. 311, 2015 to Xinjian Zhu).

Reference

Banes AK, Shaw SM, Tawfik A, Patel BP, Ogbi S, Fulton D, Marrero MB (2005) Activation of the JAK/STAT pathway in vascular smooth muscle by serotonin. Am J Physiol Cell Physiol 288:C805-812.

Becker A, Grecksch G, Schroder H (1995) N omega-nitro-L-arginine methyl ester interferes with pentylenetetrazol-induced kindling and has no effect on changes in glutamate binding. Brain Res 688:230-232.

Bedard K, Krause KH (2007) The NOX family of ROS-generating NADPH oxidases: physiology and pathophysiology. Physiol Rev 87:245-313.

Bedard K, Lardy B, Krause KH (2007) NOX family NADPH oxidases: not just in mammals. Biochimie 89:1107-1112.

Brennan AM, Suh SW, Won SJ, Narasimhan P, Kauppinen TM, Lee H, Edling Y, Chan PH, Swanson RA (2009) NADPH oxidase is the primary source of superoxide induced by NMDA receptor activation. Nat Neurosci 12:857-863.

Cao L, Xu J, Lin Y, Zhao X, Liu X, Chi Z (2009) Autophagy is upregulated in rats with status epilepticus and partly inhibited

by Vitamin E. Biochem Biophys Res Commun 379:949-953.

Chu CT (2006) Autophagic stress in neuronal injury and disease. J Neuropathol Exp Neurol 65:423-432.

Crighton D, Wilkinson S, O'Prey J, Syed N, Smith P, Harrison PR, Gasco M, Garrone O, Crook T, Ryan KM (2006) DRAM, a p53-induced modulator of autophagy, is critical for apoptosis. Cell 126:121-134.

Degterev A, Huang ZH, Boyce M, Li YQ, Jagtap P, Mizushima N, Cuny GD, Mitchison TJ, Moskowitz MA, Yuan JY (2005) Chemical inhibitor of nonapoptotic cell death with therapeutic potential for ischemic brain injury (vol 1, pg 112, 2005). Nat Chem Biol 1.

Di Maio R, Mastroberardino PG, Hu X, Montero L, Greenamyre JT (2011) Pilocapine alters NMDA receptor expression and function in hippocampal neurons: NADPH oxidase and ERK1/2 mechanisms. Neurobiol Dis 42:482-495.

Espert L, Denizot M, Grimaldi M, Robert-Hebmann V, Gay B, Varbanov M, Codogno P, Biard-Piechaczyk M (2006) Autophagy is involved in T cell death after binding of HIV-1 envelope proteins to CXCR4. J Clin Invest 116:2161-2172.

Essick EE, Sam F (2010) Oxidative stress and autophagy in cardiac disease, neurological disorders, aging and cancer. Oxid Med Cell Longev 3:168-177.

Groemping Y, Rittinger K (2005) Activation and assembly of the NADPH oxidase: a structural perspective. Biochem J 386:401-416.

Hara T, Nakamura K, Matsui M, Yamamoto A, Nakahara Y, Suzuki-Migishima R, Yokoyama M, Mishima K, Saito I, Okano H, Mizushima N (2006) Suppression of basal autophagy in neural cells causes neurodegenerative disease in mice. Nature 441:885-889.

Huang J, Brumell JH (2009) NADPH oxidases contribute to autophagy regulation. Autophagy 5:887-889.

Huang J, Canadien V, Lam GY, Steinberg BE, Dinauer MC, Magalhaes MA, Glogauer M, Grinstein S, Brumell JH (2009) Activation of antibacterial autophagy by NADPH oxidases. Proc Natl Acad Sci U S A 106:6226-6231.

Itoh T, Ito Y, Ohguchi K, Ohyama M, Iinuma M, Otsuki Y, Nozawa Y, Akao Y (2008) Eupalinin A isolated from Eupatorium chinense L. induces autophagocytosis in human leukemia HL60 cells.

Bioorg Med Chem 16:721-731.

Kabeya Y, Mizushima N, Ueno T, Yamamoto A, Kirisako T, Noda T, Kominami E, Ohsumi Y, Yoshimori T (2000) LC3, a mammalian homologue of yeast Apg8p, is localized in autophagosome membranes after processing. EMBO J 19:5720-5728.

Kim JH, Jang BG, Choi BY, Kim HS, Sohn M, Chung TN, Choi HC, Song HK, Suh SW (2013) Post-treatment of an NADPH oxidase inhibitor prevents seizure-induced neuronal death. Brain Res 1499:163-172.

Klionsky DJ (2005) The molecular machinery of autophagy: unanswered questions. J Cell Sci 118:7-18.

Koike M, Shibata M, Tadakoshi M, Gotoh K, Komatsu M, Waguri S, Kawahara N, Kuida K, Nagata S, Kominami E, Tanaka K, Uchiyama Y (2008) Inhibition of autophagy prevents hippocampal pyramidal neuron death after hypoxic-ischemic injury. Am J Pathol 172:454-469.

Komatsu M, Waguri S, Chiba T, Murata S, Iwata J, Tanida I, Ueno T, Koike M, Uchiyama Y, Kominami E, Tanaka K (2006a) Loss of autophagy in the central nervous system causes

neurodegeneration in mice. Nature 441:880-884.

Komatsu M, Waguri S, Chiba T, Murata S, Iwata J, Tanida I, Ueno T, Koike M, Uchiyama Y, Kominami E, Tanaka K (2006b) Loss of autophagy in the central nervous system causes neurodegeneration in mice. Nature 441:880-884.

Komatsu M, Waguri S, Ueno T, Iwata J, Murata S, Tanida I, Ezaki J, Mizushima N, Ohsumi Y, Uchiyama Y, Kominami E, Tanaka K, Chiba T (2005) Impairment of starvation-induced and constitutive autophagy in Atg7-deficient mice. Journal of Cell Biology 169:425-434.

Kovac S, Domijan AM, Walker MC, Abramov AY (2014) Seizure activity results in calcium- and mitochondria-independent ROS production via NADPH and xanthine oxidase activation. Cell Death Dis 5:e1442.

Lai YC, Hickey RW, Chen YM, Bayir H, Sullivan ML, Chu CT, Kochanek PM, Dixon CE, Jenkins LW, Graham SH, Watkins SC, Clark RSB (2008) Autophagy is increased after traumatic brain injury in mice and is partially inhibited by the antioxidant gamma-glutamylcysteinyl ethyl ester. J Cerebr Blood F Met 28:540-550.

Lambeth JD (2004) NOX enzymes and the biology of reactive oxygen. Nat Rev Immunol 4:181-189.

Lee J, Giordano S, Zhang J (2012) Autophagy, mitochondria and oxidative stress: cross-talk and redox signalling. Biochem J 441:523-540.

Levine B, Klionsky DJ (2004) Development by self-digestion: molecular mechanisms and biological functions of autophagy. Dev Cell 6:463-477.

Levine B, Kroemer G (2008) Autophagy in the pathogenesis of disease. Cell 132:27-42.

Liang LP, Patel M (2004) Mitochondrial oxidative stress and increased seizure susceptibility in Sod2(-/+) mice. Free Radic Biol Med 36:542-554.

Martin DN, Baehrecke EH (2004) Caspases function in autophagic programmed cell death in Drosophila. Development 131:275-284.

McMahon J, Huang X, Yang J, Komatsu M, Yue Z, Qian J, Zhu X, Huang Y (2012) Impaired autophagy in neurons after disinhibition of mammalian target of rapamycin and its contribution to epileptogenesis. J Neurosci 32:15704-15714.

Mizoguchi H, Nakade J, Tachibana M, Ibi D, Someya E, Koike H, Kamei H, Nabeshima T, Itohara S, Takuma K, Sawada M, Sato J, Yamada K (2011) Matrix metalloproteinase-9 contributes to kindled seizure development in pentylenetetrazole-treated mice by converting pro-BDNF to mature BDNF in the hippocampus. J Neurosci 31:12963-12971.

Mizushima N, Yamamoto A, Matsui M, Yoshimori T, Ohsumi Y (2004) In vivo analysis of autophagy in response to nutrient starvation using transgenic mice expressing a fluorescent autophagosome marker. Mol Biol Cell 15:1101-1111.

Nauseef WM (2008) Biological roles for the NOX family NADPH oxidases. J Biol Chem 283:16961-16965.

Noh KM, Koh JY (2000) Induction and activation by zinc of NADPH oxidase in cultured cortical neurons and astrocytes. J Neurosci 20:RC111.

Ohsumi Y (2001) Molecular dissection of autophagy: two ubiquitin-like systems. Nat Rev Mol Cell Biol 2:211-216.

Patel M, Li QY, Chang LY, Crapo J, Liang LP (2005) Activation of NADPH oxidase and extracellular superoxide production in

seizure-induced hippocampal damage. J Neurochem 92:123-131.

Peker E, Oktar S, Ari M, Kozan R, Dogan M, Cagan E, Sogut S (2009) Nitric oxide, lipid peroxidation, and antioxidant enzyme levels in epileptic children using valproic acid. Brain Res 1297:194-197.

Pestana RR, Kinjo ER, Hernandes MS, Britto LR (2010) Reactive oxygen species generated by NADPH oxidase are involved in neurodegeneration in the pilocarpine model of temporal lobe epilepsy. Neurosci Lett 484:187-191.

Rangaraju S, Verrier JD, Madorsky I, Nicks J, Dunn WA, Jr., Notterpek L (2010) Rapamycin activates autophagy and improves myelination in explant cultures from neuropathic mice. J Neurosci 30:11388-11397.

Rowley S, Liang LP, Fulton R, Shimizu T, Day B, Patel M (2015) Mitochondrial respiration deficits driven by reactive oxygen species in experimental temporal lobe epilepsy. Neurobiol Dis 75:151-158.

Rubinsztein DC, DiFiglia M, Heintz N, Nixon RA, Qin ZH, Ravikumar B, Stefanis L, Tolkovsky A (2005) Autophagy and

its possible roles in nervous system diseases, damage and repair. Autophagy 1:11-22.

Ryan K, Backos DS, Reigan P, Patel M (2012) Post-translational oxidative modification and inactivation of mitochondrial complex I in epileptogenesis. J Neurosci 32:11250-11258.

Ryan K, Liang LP, Rivard C, Patel M (2014) Temporal and spatial increase of reactive nitrogen species in the kainate model of temporal lobe epilepsy. Neurobiol Dis 64:8-15.

Ryter SW, Nakahira K, Haspel JA, Choi AM (2012) Autophagy in pulmonary diseases. Annu Rev Physiol 74:377-401.

Scherz-Shouval R, Elazar Z (2007) ROS, mitochondria and the regulation of autophagy. Trends Cell Biol 17:422-427.

Scherz-Shouval R, Elazar Z (2011) Regulation of autophagy by ROS: physiology and pathology. Trends Biochem Sci 36:30-38.

Scherz-Shouval R, Shvets E, Fass E, Shorer H, Gil L, Elazar Z (2007) Reactive oxygen species are essential for autophagy and specifically regulate the activity of Atg4. EMBO J 26:1749-1760.

Schroder H, Becker A, Lossner B (1993) Glutamate binding to brain membranes is increased in pentylenetetrazole-kindled rats. J Neurochem 60:1007-1011.

Shacka JJ, Lu J, Xie ZL, Uchiyama Y, Roth KA, Zhang J (2007) Kainic acid induces early and transient autophagic stress in mouse hippocampus. Neurosci Lett 414:57-60.

Shintani T, Klionsky DJ (2004) Autophagy in health and disease: a double-edged sword. Science 306:990-995.

Siebel AM, Menezes FP, da Costa Schaefer I, Petersen BD, Bonan CD (2015) Rapamycin suppresses PTZ-induced seizures at different developmental stages of zebrafish. Pharmacol Biochem Behav.

Sosanya NM, Brager DH, Wolfe S, Niere F, Raab-Graham KF (2015) Rapamycin reveals an mTOR-independent repression of Kv1.1 expression during epileptogenesis. Neurobiol Dis 73:96-105.

Tammariello SP, Quinn MT, Estus S (2000) NADPH oxidase contributes directly to oxidative stress and apoptosis in nerve growth factor-deprived sympathetic neurons. J Neurosci 20:RC53.

Tejada-Simon MV, Serrano F, Villasana LE, Kanterewicz BI, Wu GY, Quinn MT, Klann E (2005) Synaptic localization of a functional NADPH oxidase in the mouse hippocampus. Mol Cell Neurosci 29:97-106.

Tsai HL, Chang CN, Chang SJ (2010) The effects of pilocarpine-induced status epilepticus on oxidative stress/damage in developing animals. Brain Dev 32:25-31.

Waldbaum S, Liang LP, Patel M (2010) Persistent impairment of mitochondrial and tissue redox status during lithium-pilocarpine-induced epileptogenesis. J Neurochem 115:1172-1182.

Zhu C, Wang X, Xu F, Bahr BA, Shibata M, Uchiyama Y, Hagberg H, Blomgren K (2005) The influence of age on apoptotic and other mechanisms of cell death after cerebral hypoxia-ischemia. Cell Death and Differentiation 12:162-176.

Zhu X, Dong J, Shen K, Bai Y, Zhang Y, Lv X, Chao J, Yao H (2015) NMDA receptor NR2B subunits contribute to PTZ-kindling-induced hippocampal astrocytosis and oxidative stress. Brain Res Bull 114:70-78.

Zhu XJ, Hua Y, Jiang J, Zhou QG, Luo CX, Han X, Lu YM, Zhu DY

(2006) Neuronal nitric oxide synthase-derived nitric oxide inhibits neurogenesis in the adult dentate gyrus by down-regulating cyclic AMP response element binding protein phosphorylation. Neuroscience 141:827-836.

Figures CAPTIONS:

Fig. 1. The PTZ-induced kindling model. Kindling was evoked by repeatedly and intermittently treating mice with PTZ at a dose of 35 mg/kg once every other day for eleven total injections, or with 35 mg/kg PTZ once every other day for six total injections. The mice showing more than three consecutive stage 4 seizures were considered to be fully kindled **($F_{1,10}$=70.5, p<0.001, n=8)**, while those showing stage 2 or stage 3 seizures were considered to be partially kindled **(n=8).** The values are the means ± S.E.M. **p<0.001 compared with vehicle control mice, repeated measures ANOVA.

Fig. 2. The expression levels of autophagy-related proteins were increased in the hippocampus of PTZ-kindled mice. (A) Western blots showing the protein levels of hippocampal LC3I,

LC3II, Beclin-1, ATG-5 and ATG-7 in the vehicle control, partially kindled and fully kindled mice. **(B-F)** Bar graphs showing the quantification of the hippocampal LC3 II (**$F_{3,16}$=13.94, *p*<0.001,** Vehicle Ctrl ***vs*** 24 hr post-kindling**; *p*<0.001,** Partially kindled *vs* 24 hr post-kindling**; *p*<0.001,** 6 hr post-kindling ***vs*** 24 hr post-kindling), Beclin-1(**$F_{3,16}$=14.86, *p*<0.001,** Vehicle Ctrl ***vs*** 24 hr post-kindling**; *p*<0.001,** Partially kindled ***vs*** 24 hr post-kindling**; *p*=0.004,** 6 hr post-kindling ***vs*** 24 hr post-kindling), ATG-5 (**$F_{3,16}$=7.62, *p*=0.006,** Vehicle Ctrl ***vs*** 6 hr post-kindling**; *p*=0.002,** Vehicle Ctrl ***vs*** 24 hr post-kindling**; *p*=0.006,** Partially kindled ***vs*** 6 hr post-kindling**; *p*=0.002,** Partially kindled ***vs*** 24 hr post-kindling), ATG-7 (**$F_{3,16}$=8.82, *p*<0.001,** Vehicle Ctrl ***vs*** 24 hr post-kindling**; *p*<0.001,** Partially kindled ***vs*** 24 hr post-kindling), LC3II/LC3I ratio (**$F_{3,16}$=11.62, *p*<0.001,** Vehicle Ctrl ***vs*** 24 hr post-kindling**; *p*<0.001,** Partially kindled ***vs*** 24 hr post-kindling), which were represented as the intensity ratios of these molecules to β-actin, or as the intensity ratio of LC3II to LC3I in the vehicle control, partially kindled and fully kindled mice **(n=5)**. The values are the means ± S.E.M. ***p*<0.01, ****p*<0.001, one-way ANOVA.

Fig. 3. PTZ kindling induced punctate LC3 accumulation and autophagosomal vacuole formation in the hippocampal CA1

region. (A-C) Representative images of the immunostaining of LC3 puncta in the hippocampal CA1 region of the vehicle control, partially kindled and fully kindled mice, respectively. **(D)** A higher magnification image of the hippocampal CA1 punctate LC3 immunostaining in fully kindled mice. Red fluorescence indicates punctate staining for LC3. Nuclei were counterstained with DAPI (blue). The arrowheads indicate LC3 accumulation. **(E)** A representative image of the LC3 puncta (Red) and NeuN (Green) co-staining in the hippocampal CA1 region of fully kindled mice. Nuclei were counterstained with DAPI (blue). The arrowheads indicate the LC3 and NeuN co-labeled cells. **(F)** The bar graph shows the quantification of the hippocampal CA1 LC3 puncta-positive cells in the vehicle control, partially kindled and fully kindled mice (**$F_{2,12}$=15.90, *p*<0.001,** Vehicle Ctrl ***vs*** Fully kindled; ***p*<0.001,** Partially kindled ***vs*** Fully kindled; ***p*=0.37,** Partially kindled ***vs*** Vehicle Ctrl**). (n=5)**. **(G-H)** Representative electron photomicrographs of the autophagosomal vacuoles formed in the hippocampal CA1 regions of the vehicle control and fully kindled mice. **(I)** Bar graph showing the quantification of the hippocampal CA1 autophagosomal vacuoles in the vehicle control, partially kindled and fully kindled mice, respectively (**$F_{2,12}$=12.35, *p*<0.001,** Fully kindled ***vs*** Vehicle Ctrl; ***p*=0.002,** Fully kindled ***vs*** Partially

kindled) **(n=5)**. **(J)** Western blots showing the protein levels of hippocampal LC3I, LC3II in PTZ-kindled and control mice which were treated with Leupeptin or saline. **(K-L)** Bar graphs showing the quantification of the hippocampal LC3 II level and the ration of LC3II/LC3I, which were represented as the intensity ratios of LC3II to β-actin, or as the intensity ratio of LC3II to LC3I in these mice. With regard to the level of LC3-II, a two-way ANOVA revealed a significant main effect of both PTZ kindling **($F_{1,16}$=13.74, *p*=0.002)** and leupeptin treatment **($F_{1,16}$=7.41, *p*=0.015)** and there was a significant interaction between PTZ kindling and leupeptin treatment **($F_{1,16}$=0.532, *p*=0.04)**. A Tukey *post-hoc* test revealed that the levels of LC3-II in leupeptin-treated mice were significantly increased compared with those in control animals **(*p*<0.05)**. PTZ-kindling resulted in an increase in LC3-II levels **(*p*<0.01)**, an effect that was augmented by leupeptin treatment **(*p*<0.05)**. With regard to the ratio of LC3-II/LC3-I, a two-way ANOVA revealed a significant main effect of both PTZ-kindling **($F_{3,12}$=5.74, *p*=0.002)** and leupeptin treatment **($F_{3,12}$=0.41, *p*<0.001)** and there was a significant interaction between PTZ kindling and leupeptin treatment **($F_{3,12}$=7.95, *p*=0.04)**. A Tukey *post-hoc* test revealed that the ratio of LC3-II/LC3-I in leupeptin-treated mice was significantly increased compared with those in control animals **(p<0.01)**,

PTZ-kindling resulted in an increase in the ratio of LC3-II/LC3-I **(*p*<0.01)**, an effect that was augmented by leupeptin treatment **(*p*<0.05).** The values are the means ± S.E.M. **p*<0.05, ***p*<0.01, ****p*<0.001, one-way or two-way ANOVA. Scale bar = 100 μm in **(A-C)**, 200 μm in **(D, E)** and 500 nm in **(G, H).**

Fig. 4. PTZ kindling induced the expression of NADPH oxidase subunit p47phox in the hippocampus. **(A)** Representative images of p47phox immunostaining and the quantification of the number of p47phox-positive cells in the hippocampal CA1 region of the vehicle control, partially kindled and fully kindled mice (**$F_{2,12}$=11.44, *p*=0.001,** Fully kindled ***vs*** Vehicle ctrl; ***p*=0.047,** Fully kindled ***vs*** Partially kindled) **(n=5)**. **(B)** Western blots showing the protein levels of hippocampal NADPH oxidase subunit p47phox, p67phox and gp91phox in the vehicle control, partially kindled and fully kindled mice. Bar graphs showing the quantifications of the hippocampal p47phox (**$F_{3,16}$=15.91, *p*<0.001,** 24 hr post-kindling ***vs*** Vehicle ctrl; ***p*<0.001,** 6 hr post-kindling ***vs*** Vehicle ctrl; ***p*<0.05,** Partially kindled ***vs*** 24 hr post-kindling), p67phox (**$F_{3,16}$=0.29, *p*=0.835**) and gp91phox (**$F_{3,16}$=0.10, *p*=0.959**) protein levels, which were represented as the intensity ratio of p47phox, p67phox and gp91phox to β-actin in the vehicle control, partially kindled and

fully kindled mice **(n=5)**. The values are the means ± S.E.M. **p*<0.05, ***p*<0.01, ****p*<0.001, one-way ANOVA.

Fig. 5. PTZ kindling-induced hippocampal ROS production and lipid peroxidation are dependent on the activation of NADPH oxidase. (A) A schematic representation of the experimental design. Mice were repeatedly treated with 35 mg/kg PTZ every other day to induce kindling. Immediately after these mice were fully kindled, they were administered apocynin at 20 mg/kg four times at six-hour intervals. These mice were then sacrificed six hours after the last apocynin injection to detect the ROS production and lipid peroxidation and for a mitochondrial ultrastructural analysis. **(B)** Representative images of DHE fluorescence in the hippocampus of the vehicle control, fully kindled, fully kindled apocynin-treated and apocynin-treated mice. **(C)** A bar graph showing the quantification of the DHE fluorescence intensity, which represents the ROS levels in the hippocampus of the vehicle control, fully kindled, fully kindled apocynin-treated and apocynin-treated mice. A two-way ANOVA revealed a significant main effect of PTZ kindling **($F_{1,16}$=42.25, *p*<0.001)** and apocynin treatment **($F_{1,16}$=12.25, *p*=0.003)** on the DHE fluorescence intensity, and there was a significant interaction between PTZ kindling and

apocynin treatment **($F_{1,16}$=12.25, *p*=0.003)**. A Tukey *post-hoc* test revealed that fully PTZ-kindled mice displayed higher DHE fluorescence intensity compared to the vehicle control mice **(*p*<0.001).** Apocynin treatment suppressed the PTZ kindling-induced increase in the DHE intensity **(*p*< 0.001)**, while the mice treated with apocynin alone did not show a significant difference in the DHE intensity compared to the vehicle control mice **(*p*= 0.59)** (n=5). **(D, E)** Bar graphs showing the quantification of the lipid peroxidation products (MDA and 4-HNE) in the hippocampus of the vehicle control, fully kindled, fully kindled apocynin-treated and apocynin-treated mice. With regard to the MDA content, A two-way ANOVA revealed a significant main effect of both PTZ kindling **($F_{1,20}$=34.46, *p*<0.001)** and apocynin treatment **($F_{1,20}$=11.67, *p*=0.003)**, and there was a significant interaction between PTZ kindling and apocynin treatment **($F_{1,20}$=8.08, *p*=0.01)**. A Tukey *post-hoc* test revealed that MDA content was significantly increased in fully PTZ-kindled mice compared to the vehicle control mice **(*p*<0.001).** Apocynin treatment suppressed the PTZ kindling-induced increase in the MDA level **(*p*< 0.001)**, while mice treated with apocynin alone did not show any significant difference in the MDA content compared to the vehicle control mice **(*p*= 0.68)**. With regard to the 4-HNE contents, A two-way ANOVA revealed a

significant main effect of both PTZ-kindling **($F_{1,20}$=23.35, *p*<0.001)** and apocynin treatment **($F_{1,20}$=9.18, *p*=0.007)** but there was no significant interaction between PTZ kindling and apocynin treatment **($F_{1,20}$=3.76, *p*=0.07)**. A Tukey *post-hoc* test revealed that 4-HNE content was significantly increased in fully PTZ-kindled mice compared to the vehicle control mice **(*p*<0.001).** Apocynin treatment suppressed the PTZ kindling-induced increase in the 4-HNE level **(*p*=0.002)**, while the mice treated with apocynin alone did not show any significant difference in the 4-HNE content compared to the vehicle control mice **(*p*=0.45)**. The values are the means ± S.E.M. ***p*<0.01, ****p*<0.001, two-way ANOVA. Scale bar=50 μm.

Fig. 6. PTZ kindling-induced hippocampal CA1 mitochondrial ultrastructural damage is dependent on the activation of NADPH oxidase. Representative electron photomicrographs of the hippocampal CA1 mitochondrial ultrastructure in vehicle control **(A),** fully kindled **(B),** fully kindled apocynin-treated **(C)** and apocynin-treated mice **(D)**. The arrowheads indicate mitochondrial swelling, which was accompanied by a disruption in the membrane integrity. Scale bar, 200 nm.

Fig. 7. PTZ kindling-induced hippocampal autophagy is dependent on the activation of NADPH oxidase. (A) A western blot showing the protein levels of hippocampal LC3I, LC3II, Beclin-1, ATG-5 and ATG-7 in vehicle control, fully kindled, fully kindled apocynin-treated and apocynin-treated mice. **(B-F)** Bar graphs showing the quantification of the hippocampal LC3II, Beclin-1, ATG-5, and ATG-7 levels, and the LC3II/LC3I ratio, which were represented as the intensity ratios of these proteins to β-actin or the intensity ratio of LC3II to LC3I in the four groups of mice. A two-way ANOVA revealed a significant main effect of PTZ kindling on the protein levels of LC3-II **($F_{1,16}$=7.76, *p*<0.013)**, Beclin-1 **($F_{1,16}$=9.16, *p*=0.008)**, ATG-5 **($F_{1,16}$=25.93, *p*<0.001)** , ATG-7 **($F_{1,16}$=13.26, *p*=0.002)** and the ratio of LC3-II/LC3-I **($F_{1,16}$=7.09, *p*=0.017)** and a significant main effect of apocynin treatment on the protein levels of LC3-II **($F_{1,16}$=8.28, *p*=0.011)**, Beclin-1 **($F_{1,16}$=3.18, *p*=0.03)**, ATG-5 **($F_{1,16}$=7.19, *p*=0.016)**, ATG-7 **($F_{1,16}$=5.73, *p*=0.029)** and the ration of LC3-II/LC3-I **($F_{1,16}$=3.55, *p*=0.008)** and there was a significant interaction between PTZ kindling and apocynin treatment on the protein level of LC3-II **($F_{1,16}$=4.07, *p*=0.02)**, Beclin-1 **($F_{1,16}$=2.15, *p*=0.012)**, ATG-5 **($F_{1,16}$=6.24, *p*<0.001)**, ATG-7 **($F_{1,16}$=4.58, *p*=0.048)** and the ratio of LC3-II/LC3-I **($F_{1,16}$=3.20, *p*=0.013)**. A Tukey *post-hoc* test revealed that apocynin treatment

significantly decreased the PTZ kindling-induced levels of the LC3-II **(*p*<0.05)**, Beclin-1 **(*p*<0.05)**, ATG-5 **(*p*<0.01),** and ATG-7 **(*p*<0.01)** proteins and the ratio of LC3-II/ LC3-I **(*p*<0.05) (n=5). (G)** Representative images of punctate LC3 immunostaining in the hippocampal CA1 region of vehicle control, fully kindled, fully kindled apocynin-treated and apocynin-treated mice, respectively. **(H)** Representative electron photomicrographs of the autophagosomal vacuole formation in the hippocampal CA1 regions of the four groups of mice. **(I)** A bar graph shows the quantification of the hippocampal CA1 LC3 puncta-positive cells in the four groups of mice. A two-way ANOVA revealed a significant main effect of PTZ kindling **($F_{1,16}$=14.46, *p*=0.002)** and apocynin treatment **($F_{1,16}$=5.81, *p*=0.028)** on the the number of LC3 puncta-positive cells and there was a significant interaction between PTZ kindling and apocynin treatment **($F_{1,16}$=4.29, *p*=0.04).** A Tukey *post-hoc* test revealed that apocynin treatment significantly decreased the number of LC3 puncta-positive cells in fully kindled mice **(*p*<0.05) (n=5)**. **(J)** A bar graph shows the quantification of the hippocampal CA1 autophagosomal vacuoles in the four groups of mice. A two-way ANOVA revealed a significant main effect of PTZ kindling **($F_{1,16}$=14.73, *p*=0.01)** and apocynin treatment **($F_{1,16}$=8.91, *p*=0.009)** on the the number of

autophagosomal vacuoles and there was a significant interaction between PTZ kindling and apocynin treatment **($F_{1,16}$=6.55, *p*=0.021)**. A Tukey *post-hoc* test revealed that apocynin significantly decreased the number of autophagosomal vacuoles in fully kindled mice **(*p*<0.01) (n=5)**. The values are the means ± S.E.M. **p*<0.05, ***p*<0.01, two-way ANOVA. Scale bar=100 μm in **(C-D)**, 500 nm in **(F, G).**

Fig. 8. Pharmacological modulation of autophagy alters PTZ-induced kindling development. (A) Mice received PTZ injection alone or Chloroquine (CQ), Apocynin, Rapamycin 30min before each PTZ injection once every other day for eleven total injections. Mice showing more than three consecutive stage 4 seizures were considered to be fully kindled (**$F_{3,30}$=22.14, *p*<0.05,** CQ+PTZ ***vs*** PTZ; ***p*<0.001,** Apocynin+PTZ ***vs*** PTZ; ***p*<0.001,** Rapamycin+PTZ ***vs*** PTZ) **(n=8).** The values are the means ± S.E.M. **p*<0.05, ***p*<0.01 compared with PTZ-injection mice, repeated measures ANOVA. **(B-D)** Bar graphs showing the quantification of the protein carbonyl content (**$F_{3,20}$=11.91, *p*<0.01,** CQ+PTZ ***vs*** PTZ; ***p*<0.05,** Rapamycin+PTZ ***vs*** PTZ; ***p*<0.05,** Apocynin+PTZ ***vs*** PTZ) and lipid peroxidation products of 4-HNE (**$F_{3,20}$=8.94, *p*<0.01,** CQ+PTZ ***vs*** PTZ; ***p*<0.05,** Rapamycin+PTZ ***vs***

PTZ; ***p*<0.05,** Apocynin+PTZ ***vs*** PTZ) and MDA (**$F_{3,20}$=3.80, *p*<0.05,** Rapamycin+PTZ ***vs*** PTZ) in the hippocampus of the PTZ, CQ+PTZ, Apocynin+PTZ and Rapamycin+PTZ mice. The values are the means±S.E.M. **p*<0.05, ***p*<0.01, two-way ANOVA.

List of figures:

Figure 1

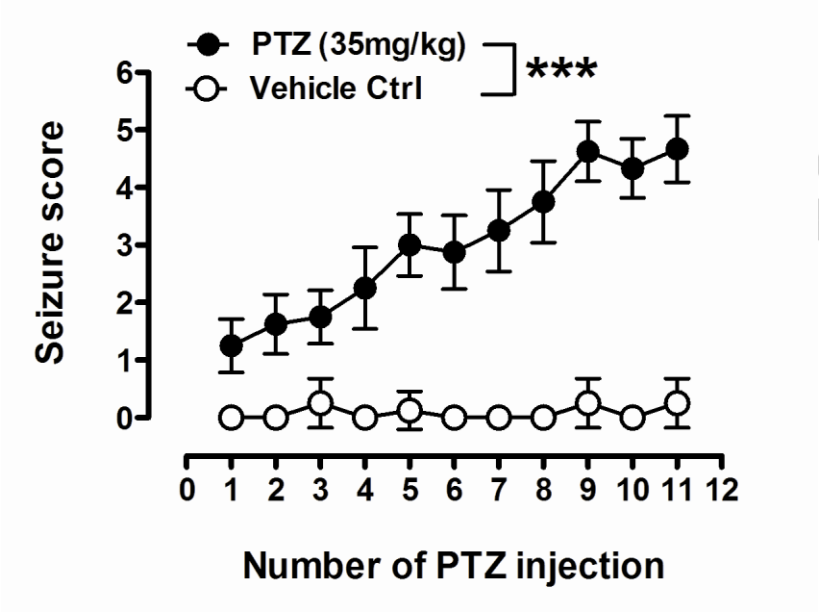

Figure 2

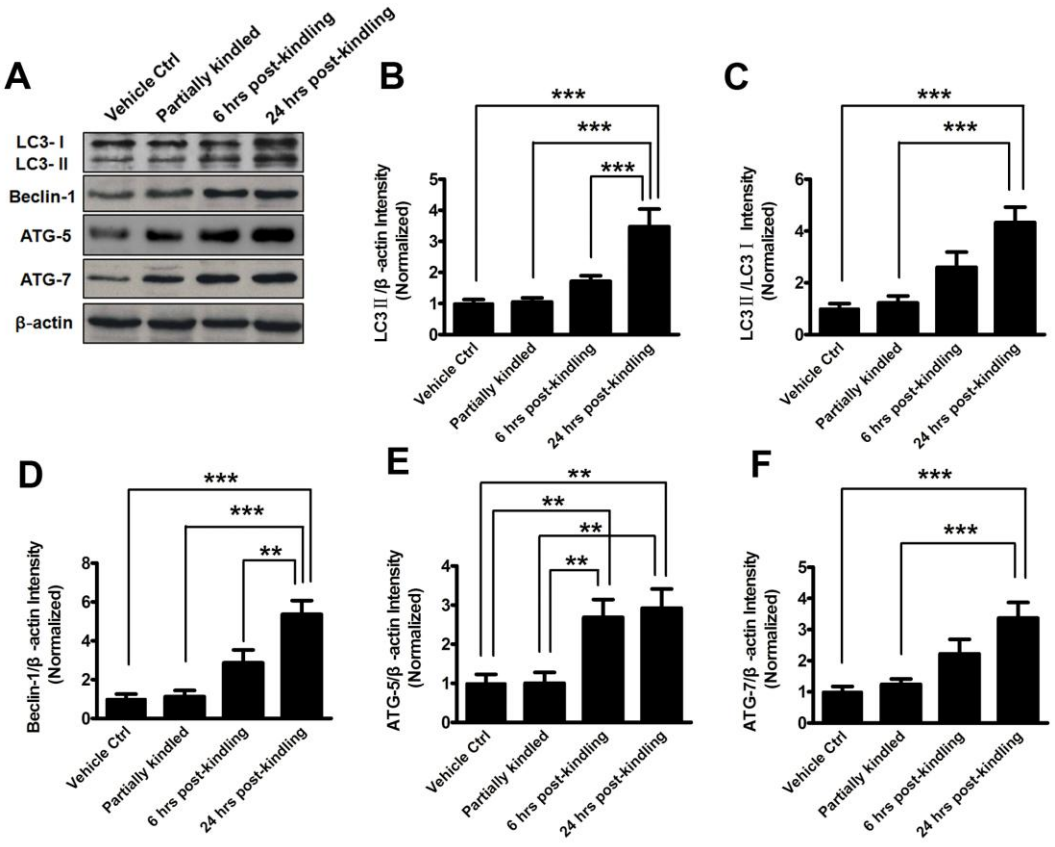

Figure 3

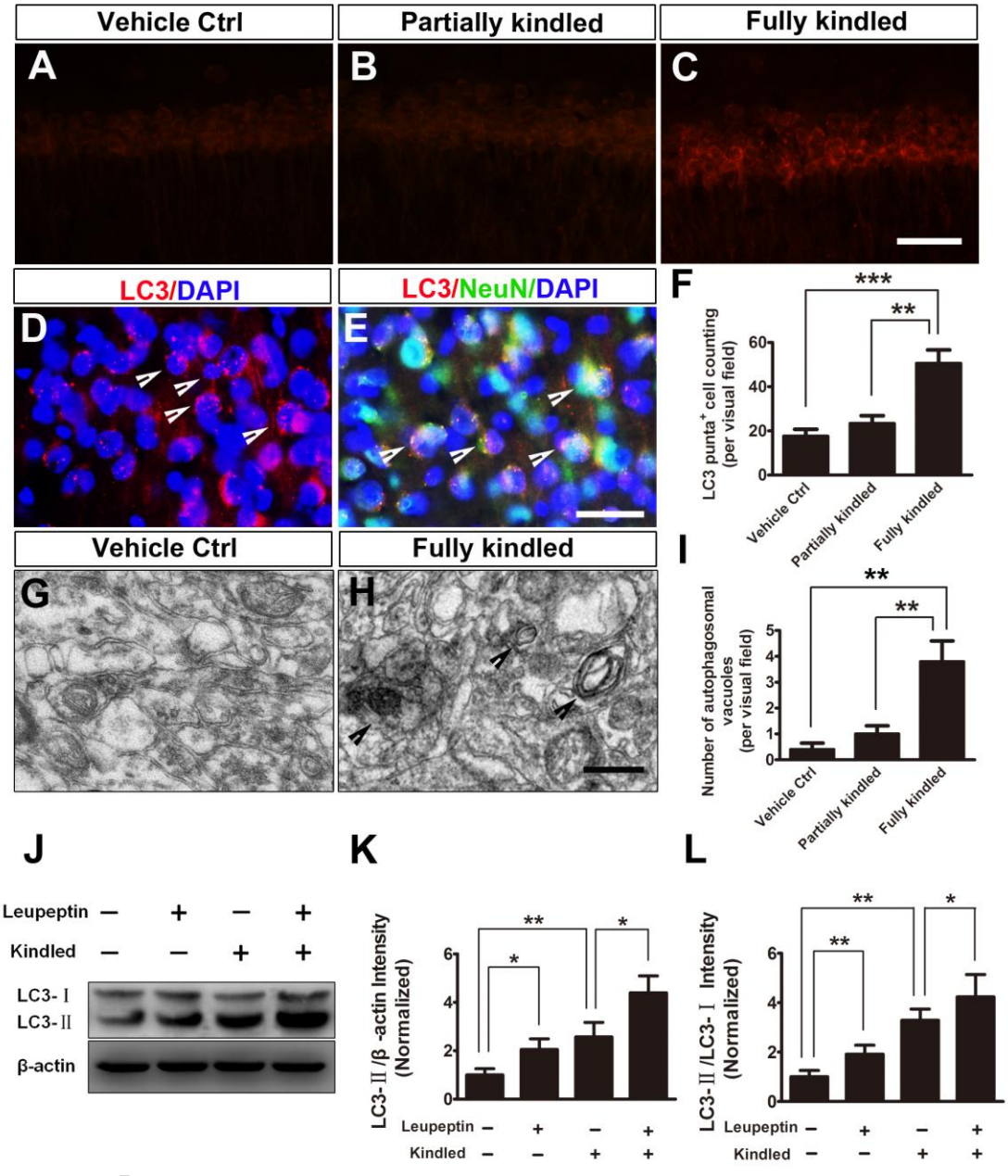
Vehicle Ctrl
Partially kindled
Fully kindled
A
B
C
LC3/DAPI
LC3/NeuN/DAPI
D
E
F
***
**
LC3 punta+ cell counting (per visual field)
60
40
20
0
Vehicle Ctrl
Partially kindled
Fully kindled
Vehicle Ctrl
Fully kindled
G
H
I
**
**
Number of autophagosomal vacuoles (per visual field)
5
4
3
2
1
0
Vehicle Ctrl
Partially kindled
Fully kindled
J
K
L
Leupeptin – + – +
Kindled – – + +
LC3-Ⅰ
LC3-Ⅱ
β-actin
**
*
LC3-Ⅱ/β -actin Intensity (Normalized)
6
4
2
0
Leupeptin – + – +
Kindled – – + +
**
*
**
LC3-Ⅱ/LC3-Ⅰ Intensity (Normalized)
6
4
2
0
Leupeptin – + – +
Kindled – – + +

Figure 4

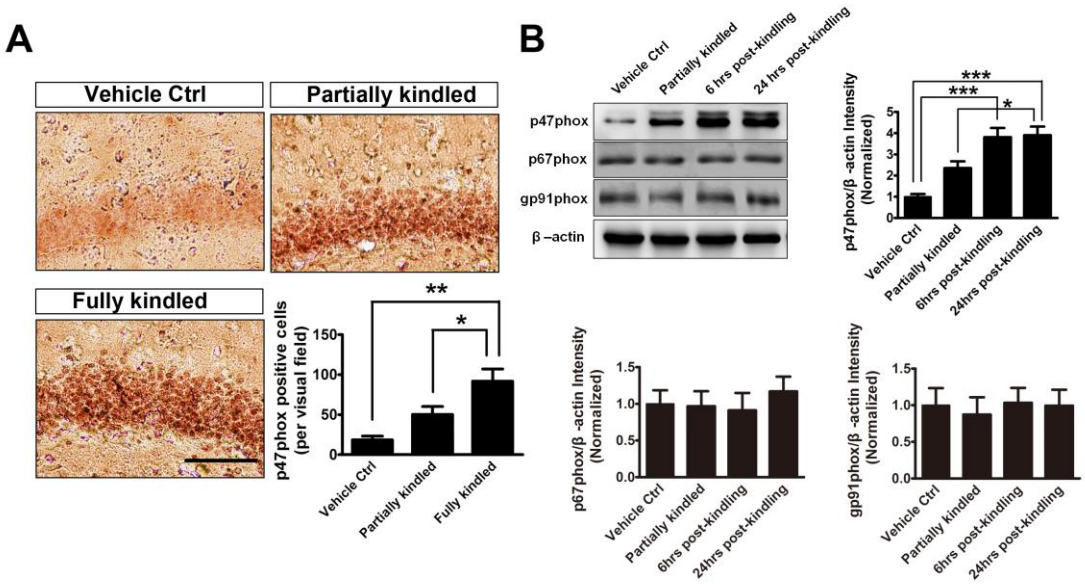

Figure 5

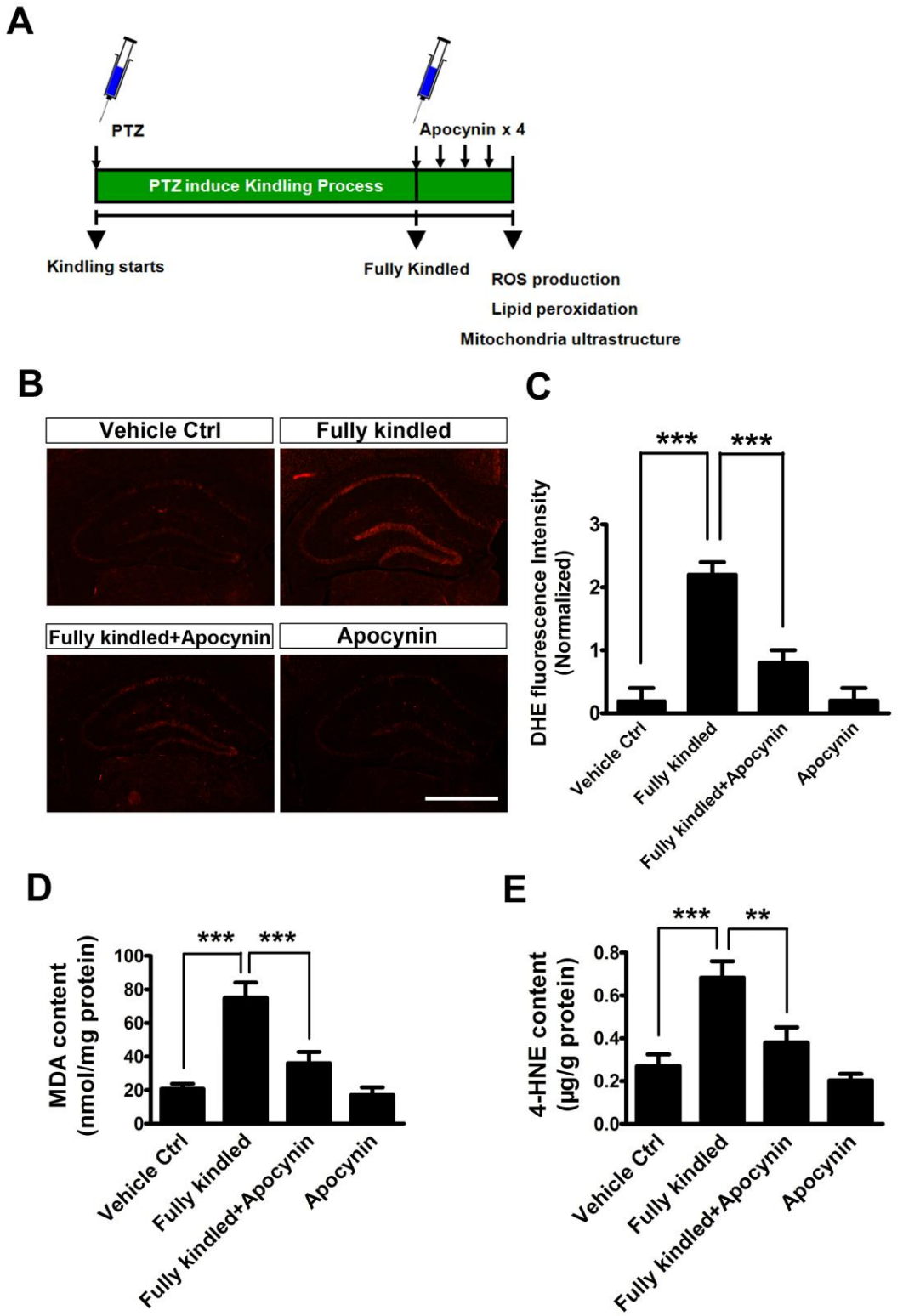
A
PTZ
Apocynin x 4
PTZ induce Kindling Process
Kindling starts
Fully Kindled
ROS production
Lipid peroxidation
Mitochondria ultrastructure
B
Vehicle Ctrl
Fully kindled
Fully kindled+Apocynin
Apocynin
C
DHE fluorescence Intensity (Normalized)
***
***
Vehicle Ctrl
Fully kindled
Fully kindled+Apocynin
Apocynin
D
MDA content (nmol/mg protein)
***
***
Vehicle Ctrl
Fully kindled
Fully kindled+Apocynin
Apocynin
E
4-HNE content (μg/g protein)
***
**
Vehicle Ctrl
Fully kindled
Fully kindled+Apocynin
Apocynin

Figure 6

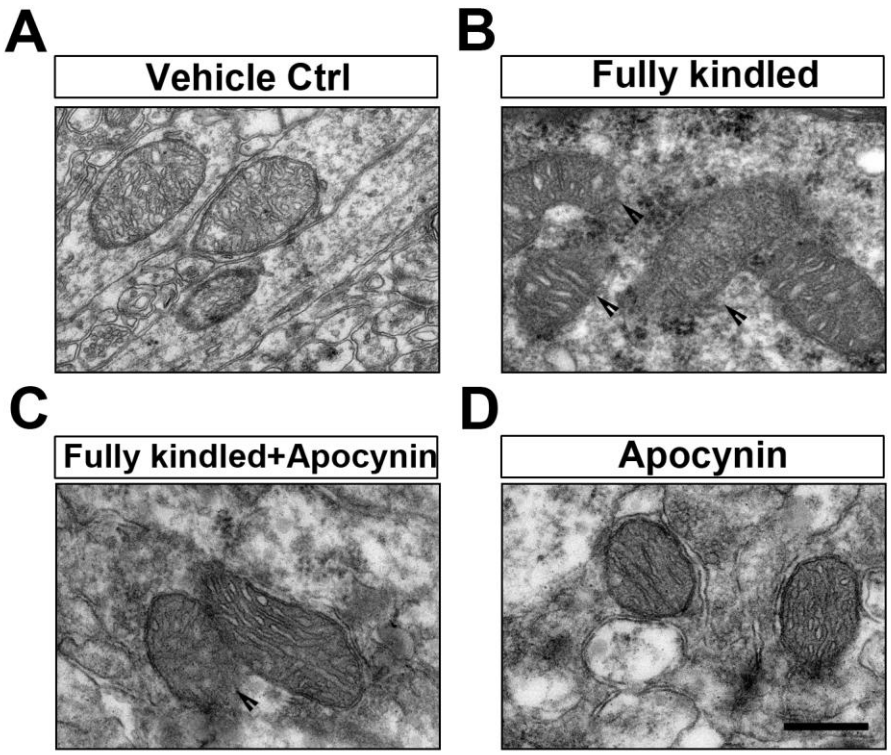

Figure 7

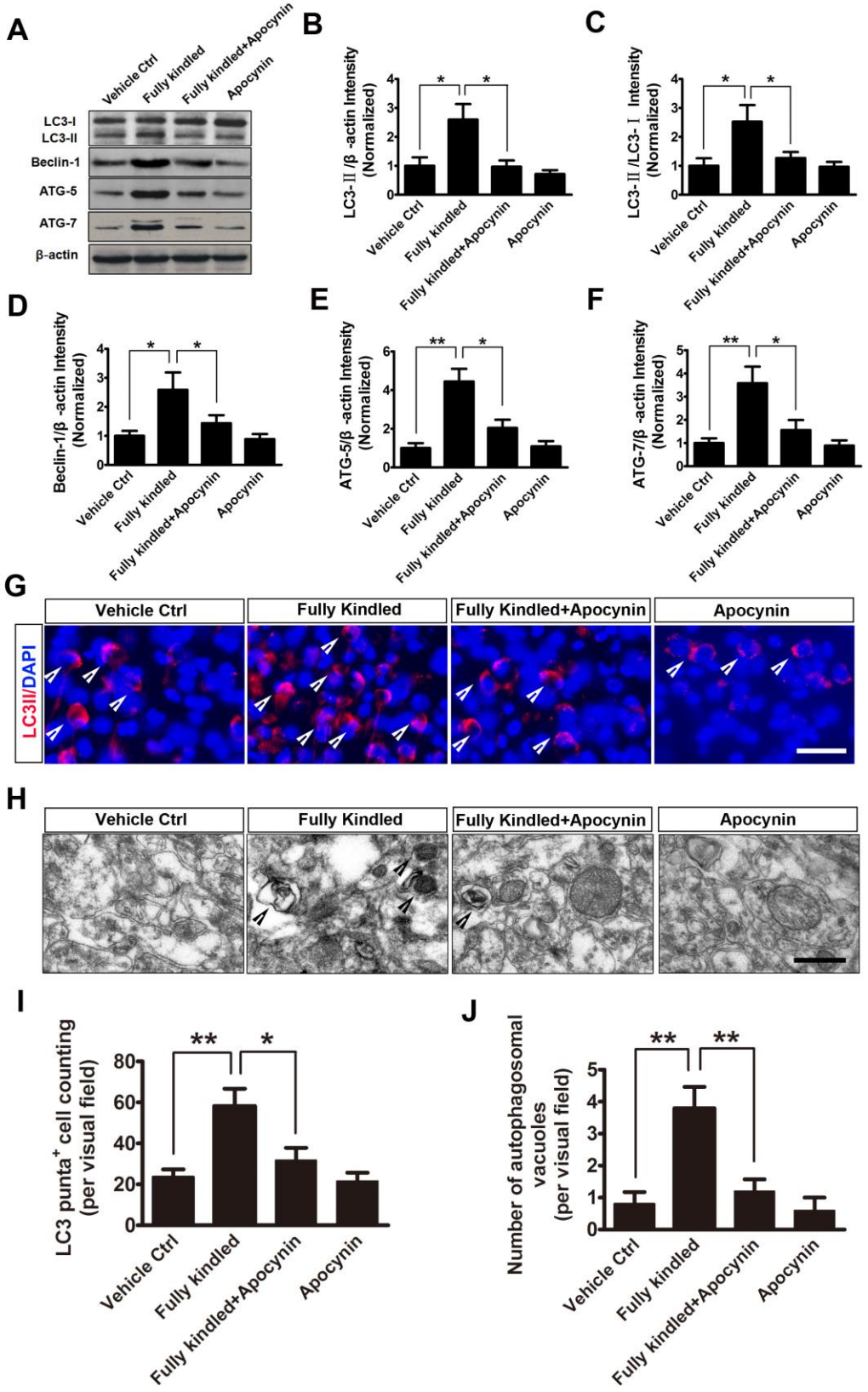
A
Vehicle Ctrl
Fully kindled
Fully kindled+Apocynin
Apocynin
LC3-I
LC3-II
Beclin-1
ATG-5
ATG-7
β-actin
B
LC3-Ⅱ/β -actin Intensity (Normalized)
C
LC3-Ⅱ/LC3-Ⅰ Intensity (Normalized)
D
Beclin-1/β -actin Intensity (Normalized)
E
ATG-5/β -actin Intensity (Normalized)
F
ATG-7/β -actin Intensity (Normalized)
G
Vehicle Ctrl
Fully Kindled
Fully Kindled+Apocynin
Apocynin
LC3II/DAPI
H
I
LC3 punta+ cell counting (per visual field)
J
Number of autophagosomal vacuoles (per visual field)

Figure 8

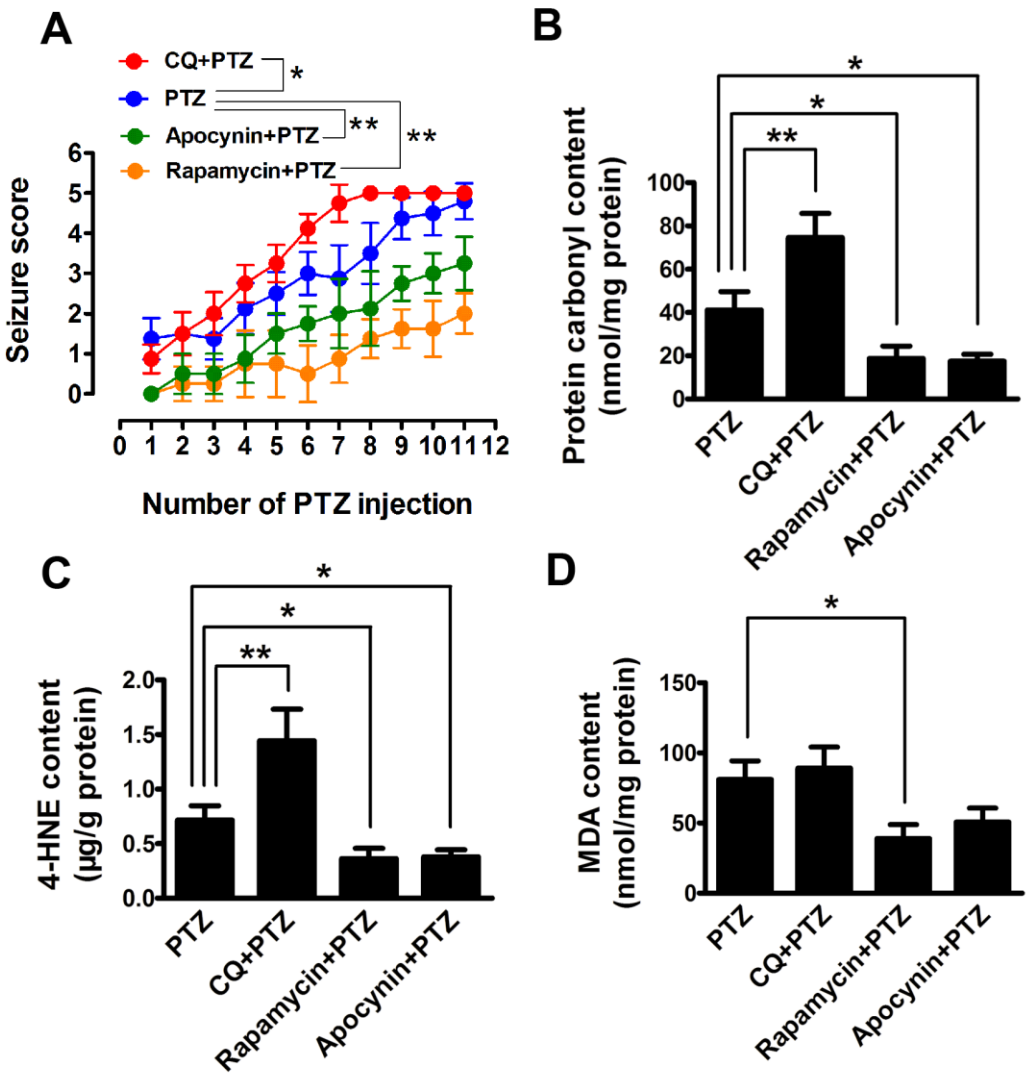
A
CQ+PTZ
PTZ
Apocynin+PTZ
Rapamycin+PTZ
*
**
**
Seizure score
0 1 2 3 4 5 6
0 1 2 3 4 5 6 7 8 9 10 11 12
Number of PTZ injection
B
Protein carbonyl content (nmol/mg protein)
0 20 40 60 80 100
PTZ
CQ+PTZ
Rapamycin+PTZ
Apocynin+PTZ
C
4-HNE content (μg/g protein)
0.0 0.5 1.0 1.5 2.0
D
MDA content (nmol/mg protein)
0 50 100 150

Highlights

- PTZ kindling enhanced autophagy level in hippocampal CA1 region
- PTZ kindling induced hippocampal NADPH oxidase activation
- PTZ kindling-induced oxidative stress is dependent on the activation of NADPH oxidase
- PTZ kindling induced mitochondrial ultrastructural damage in hippocampal CA1 region is dependent on the activation of NADPH oxidase
- PTZ kindling-induced hippocampal autophagy is dependent on the activation of NADPH oxidase